Convective variability in real mid-latitude weather: Which model best explains it?

September 20, 2016

Contents

1 Introduction

1.1 The cumulus parameterization problem

Effect of unresolved scales on the resolved scales is described by finding a simple model of what the unresolved scales do given some resolved parameters. In mass flux schemes typically a closure assumption is used to determine the mean mass flux, which is then used in a cloud model to determine the heating rate, etc.

If many small scale features are in the LS box, this approximation can be done almost deterministically, but as the grid sizes get smaller, the sampling issue and therefore the fluctuations around the mean state become significant (when is mean eq std?). In these cases deterministic parameterizations can lead to systematic biases and underrepresentations of extremes. Stochastic parameterizations aim to randomly chose one small scale state compatible with the large scale. The goal is to find a model for the variability around the mean response.

Schematic diagram.

1.2 The Craig and Cohen (2006) theory and its application in Plant and Craig (2008)

The Craig and Cohen (2006)(CC06) theory aims to quantify the mass flux fluctuations of a cloud field in convective equilibrium. Convective equilibrium implies that the average properties of the convection are determined by the large-scale forcing. In more detail, the average total mass flux $\langle M \rangle$ is a function of the large-scales. Other assumptions are: (a) the mean mass flux per cloud $\langle m \rangle$ does not depend on the large-scale forcing, only the mean number of clouds $\langle N \rangle$ does; (b) non-interacting clouds: Cloud are spatially separated (no clustering) and do not influence each other. (c) Equal a priori probabilities: This statistical equilibrium assumption implies that "that clouds are equally likely to occur in any location and with any mass flux". Using these arguments as a basis, a statistical theory is constructed for the distributions of N and m:

$$P(N) = \frac{\langle N \rangle^N}{N!} e^{-\langle N \rangle} \tag{1}$$

$$P(m) = \frac{1}{\langle m \rangle} e^{-m/\langle m \rangle} \tag{2}$$

Combing these, the distribution of the total mass flux M is given by

$$P(M) = \left(\frac{\langle N \rangle}{\langle m \rangle} \right)^{1/2} e^{-\langle N \rangle} M^{-1/2} e^{-M/\langle m \rangle} I_1 \left[2 \left(\frac{\langle N \rangle}{\langle m \rangle} M \right)^{1/2} \right], \tag{3}$$

where $I_1(x)$ is the modified Bessel function of order 1. For large (small) values of $\langle N \rangle$ the shape of this function resembles a Gaussian (Poisson) distribution. It is also possible to derive an equation for the normalized variance of M:

$$\mu_2 = \frac{\langle (\delta M)^2 \rangle}{\langle M \rangle^2} = \frac{2}{\langle N \rangle} \tag{4}$$

Always note that $\langle M \rangle = \langle N \rangle \langle m \rangle$. Eq. 4 can be derived directly from Eq. 3 or from the theory of random sums (Taylor and Karlin, 1998, p.70ff): Assume $X = \xi_1 + ... + \xi_N$ where ξ_k and N have the finite moments $E[\xi_k] = \mu$, $Var[\xi_k] = \sigma^2$ and $E[N] = \nu$, $Var[N] = \tau^2$. Then the first and second moment of X are $E[X] = \mu\nu$, $Var[X] = \nu\sigma^2 + \mu^2\tau^2$.

The theoretical predictions above were tested against numerical simulations in radiative-convective equilibrium (RCE) by Cohen and Craig (2006). The results of these simulations agreed well with the theory. The error in μ_2 is around 10%, with $\mu_2\langle N \rangle \approx 1.6$. Other studies introduced time-varying forcings and looked at the differences in mass flux statistics as described below.

In the Plant and Craig (2008)(PC08) stochastic parameterization approach, the exponential m distribution (Eq. 2) is used to create a random population of plumes for each grid-box consistent with a large scale $\langle M \rangle$. From this distribution the large-scale tendencies are then computed as the sum of the cloud model output for each plume. $\langle m \rangle = 2 \times 10^7 \text{kg s}^{-1}$ is assumed to be a constant. This assumption is motivated by RCE simulations (e.g. Cohen and Craig, 2006). The theoretical prediction for the variance of M (Eq. 4) is not explicitly used in PC08, but comes from the exponential m distribution combined with the random initiation of new clouds. The cloud life time is set to 45 minutes for all clouds.

The PC08 scheme has been tested in a GCM study with some success, improving the precipitation patterns and equatorial waves (Wang et al., 2016).

1.2.1   Deviations from theory in other studies

Two studies looked at the deviations from the CC06 predictions in their simulations of convection with a time varying forcing: Davies (2008) and Davoudi et al. (2010). A quick definition of clustering for this text: Clustering describes the increased probability of occurrence of clouds near already existing clouds. So basically a spike in an RDF.

Davies (2008)   She used a model with 1km resolution, a prescribed radiative cooling and time-varying surface fluxes or temperature. The domain size was $64\,\text{km}$ by $64\,\text{km}$. For the reference RCE simulation she found $\mu_2\langle N \rangle \approx 1.5$ at 3 km, a deviation of 10% in μ_2, which is in agreement with CC06. When looking at their time-varying simulations, they see that μ_2 is increased (about 2.2) 1h after convection is first triggered and at around 15UTC. They find that at the triggering time and at 18UTC there is strong clustering at scales from 5–20 km. At the time of maximum convection (12UTC), the RDF is almost uniform and $\mu_2 \approx 0.7$. She argues that the deviation from the predicted variance can be largely explained by clustering (see Fig. 1).

Davoudi et al. (2010)   They used a similar model setup to CC06, but with a diurnal cycle through interactive radiation with fixed SST. In their Fig. 13, they show their values of $\mu_2\langle N \rangle$ for different heights. They find that for $z < 8$ km, this value is less than two. Additionally, in their Fig. 12. they plot histograms of $P(M)$ from their data. They then fit Eq. 3 with $\langle M \rangle$ and $\langle N \rangle$ as free parameters. When they compare these fitted values to the calculated values of $\langle M \rangle$ and $\langle N \rangle$ from their data, they find that $\langle M \rangle$ is similar but the fitted $\langle N \rangle$ is larger than the observed $\langle N \rangle$. They state that "Therefore, predictions of μ_2 are smaller than the corresponding normalized variance from the data. Figure 13

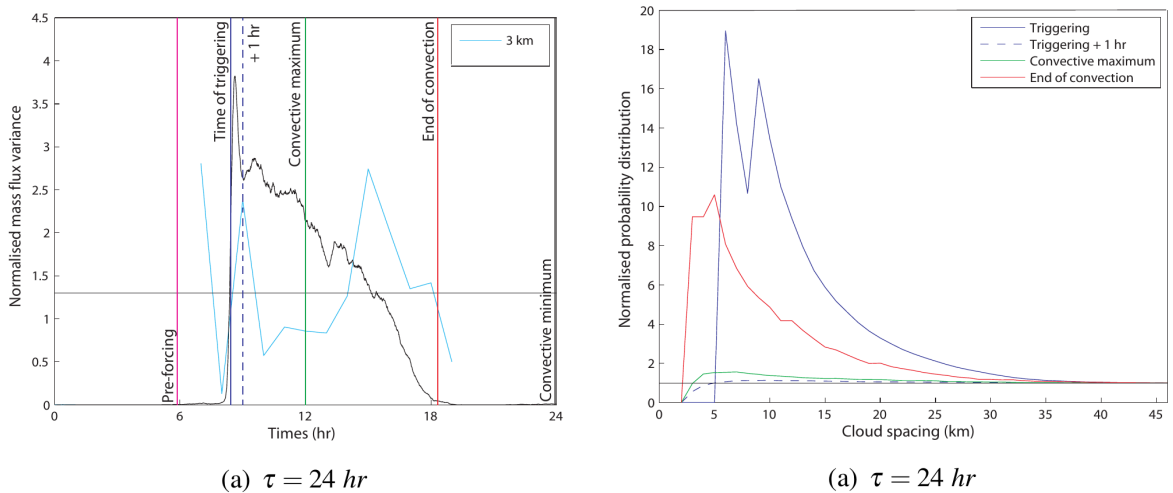<div align="center">(a) $\tau = 24\ hr$ (a) $\tau = 24\ hr$</div>

Figure 1: From Davies (2008): (left) μ_2 from their 24 h time-varying forcing simulation at a height of 3 km (blue). The black line shows the domain total mass flux at that level. (right) The corresponding RDF for the times indicated (left).

demonstrates that the variance, as well as skewness, is underestimated by the theory close to the cloud base and for the range of altitudes in $z \in [2, 8]$ km." *This statement seems wrong. Shouldn't it be the other way around? I sent them an email.*

They then look at two clustering metrics. First, the radial distribution function (their Fig. 14), where they find strong clustering for 5-10 km. Second, $\alpha = \frac{\sigma_N^2}{\langle N \rangle}$ (their Fig. 14), where they find values of about 110% at cloud base, which is in agreement with the findings by CC06 and Davies (2008).

1.3 SPPT

SPPT acts on the output of all parameterizations in the model on the assumption that the standard deviation is proportional to the mean tendencies, in case of convection this would be the heating rate (and moisture?) (cite Christensen).

1.4 Other approaches

Several approaches to get a physical model of the underlying uncertainty of convection have been tried. Dorrestijn et al. (2015) and Gottwald et al. (2016) used conditional Markov chains to describe the transition of cloud states. Bengtsson et al. (2013) used cellular automata.

Dorrestijn et al. (2015) and Gottwald et al. (2016) used conditional Markov chains to describe the transition from one cloud-state to another for several micro-nodes in a GCM grid box. The transition probabilities are dependent on some large scale indicator, in their case the large scale vertical velocity, and the exact values are calculated from observations. This approach allows them to calculate a fraction of deep convective clouds for each grid-box, which can then be used to estimate mass flux for use in a convective parameterization. The advantage of using conditional Markov chains is that they inherently have memory.

<div align="center">4</div>

Application in a simple GCM shows improvements in the distribution of precipitation, and some improvements for equatorial waves (Dorrestijn et al., 2016).

1.5   Research question / Aim of this study

The primary goal of this paper is to use a novel technique to characterize the relationship between convective variability and the mean state in real mid-latitude weather situations. How this was achieved is outlined in Section ???. The results from these numerical experiments will then be compared to the simple models of CC06 and SPPT, and we will try to find explanations for the deviations. Based on these findings we will try to use a more appropriate model and lastly investigate how this could be used to improve parameterizations.

2   Numerical experiments and case studies

The aim is to create an ensemble of simulations of real mid-latitude weather in which the large-scale conditions are sufficiently similar, but the convective clouds have been completely displaced. The first condition is achieved by using the same initial and boundary condition for each ensemble member. To fulfill the second condition a stochastic boundary layer perturbation scheme is used. The model and the boundary layer scheme will be described now.

2.1   Model description and set-up

The model used is the COSMO model (?) with 2.8 km horizontal grid spacing Δx and operational COSMO-DE settings (?) with one exception, the stochastic boundary-layer scheme which will be described below. The model does not parameterize deep convection, but a parameterization for shallow convection is included. The domain size is 357 grid points in either direction with the domain centered at 10E and 50N. For the analysis a 256 by 256 grid point domain (roughly 717km) at the center of the simulation domain is considered. The 50 grid point gap to the boundary ensures that boundary effects are minimal.

Initial and boundary conditions are taken from the operational COSMO-EU (7km) deterministic forecast (?) with a boundary condition update frequency of 1 h. All runs are started at 00UTC with a lead time of 24 h. A 50 member ensemble is created by setting a different random number seed in the stochastic boundary-layer scheme for each member. The first three hours are excluded from all analyses to allow for spin up of the simulations and perturbations, so that the analysis starts at 03UTC and ends at 24UTC. The output was available every 30 minutes. To approximate the convective heating rate Q the instantaneous microphysical temperature tendencies were used.

2.2   The PSPturb turbulence scheme

The physically-based stochastic perturbation boundary-layer scheme (PSPturb) is described and tested in Kober et al. (2016)(KC16). A brief outline is given here now. The

PSPturb scheme is an additive perturbation scheme:

$$\left(\frac{\partial \Phi}{\partial t}\right)_{\text{total}} = \left(\frac{\partial \Phi}{\partial t}\right)_{\text{parameterized}} + \eta \sigma_{\left(\frac{\partial \Phi}{\partial t}\right)_{\text{parameterized}}} \tag{5}$$

These perturbations (last term) are process-specific, so for each parameterized process the perturbations have to be calculated separately. The last term in the equation above contains a random number $\eta = N(0,1)$ and the standard deviation σ of the parameterized tendencies. The random number field has a horizontal correlation length of $5\Delta x$, the effective resolution and is held constant for 10 minutes and then drawn again from scratch. This represents a typical eddy turnover time in the boundary layer. In KC16 the standard deviation term is approximated by

$$\sigma_{\left(\frac{\partial \Phi}{\partial t}\right)_{\text{parameterized}}} = \alpha_{\text{const},\Phi} \frac{l_\infty}{5\Delta x} \frac{1}{dt} \sigma_\Phi, \tag{6}$$

where $l_\infty = 150$ m is the mixing length describing the average size of an eddy. The term σ_Φ is the sub-grid scale standard deviation. For the turbulence perturbations the considered variables are vertical velocity w, potential temperature θ and humidity q. The standard deviations are calculated in the turbulence parameterization (see KC06 for details). The factor $\frac{l_\infty}{5\Delta x} \propto \frac{1}{\sqrt{N_{\text{eddy}}}}$ scales the variability according to number of unresolved eddies similar to Eq. 4. The factor $\frac{1}{dt}$ converts the term into a tendency term dependent on the time step. Finally, a scaling factor $\alpha_{\text{const},\Phi}$ is included for tuning purposes and should be of order one. It is set to 2 for these experiments.

Fig. 2 shows the precipitation fields for three ensemble members. On the large scales the members agree on the location of the precipitation, but zooming in on the convection itself reveals no perceptible correlation.

2.3   Simulation period

The simulations were run for a continuous 12 day period from 28 May – 8 June 2016 which was characterized by strong convective rainfall over Central Europe (ask Christian for a review of this period). For a large portion of this period a low pressure system was stationed over the Central Alpine region causing South-Easterly advection over Germany. The precipitation largely followed a typical diurnal cycle (Fig. 3), along with a build up of convective available potential energy (CAPE) in the morning and growing boundary layer. The convective adjustment time scale τ_c, a measure of the synoptic forcing, shows intermediate values of around 5 h indicating moderate synoptic forcing, typical for the scattered convection seen in most of the simulated days (for an introduction to τ_c see Done et al. (2006), for a recent paper describing the calculation method used here see Flack et al. (2016)). Overall the days are very similar.

3   Calculation of statistics

Using the output from the numerical simulations statistics of the of mass flux M and heating rate Q are computed.

3.1 Mass flux M

The vertical mass flux is defined as the mass of air crossing a certain horizontal area per unit time. Since our interest is in the convective mass flux, we first have to identify the convective clouds (for an illustration of the process see Fig. 4). To do this we follow Cohen and Craig (2006) and many other previous and subsequent studies by creating a binary cloud/no cloud field using a threshold for vertical velocity $w > 1$ m s^{-1} combined with a positive cloud water content $q_c > 0$ kg kg^{-1}. By doing this we aim to identify convective updrafts, ignoring downdrafts.

Parameterizations are based on an updraft M_b, right? So if we want to test the input for the parameterization, the updrafts are what we want to look at right?

As a next step, Contiguous areas are then identified as clouds using a 4-point segmentation algorithm so that only pixels which share an edge are considered as contiguous clouds. Additionally, "overlapping" clouds are identified with the local maximum method, followed by a watershed algorithm to find the extent of each separated cloud (**?**).

For each identified cloud $k = 1, ..., N_{\text{cld},i}$ in each ensemble member $i = 1, ..., N_{\text{ens}}$ a cloud size σ_k is determined as

$$\sigma_k = N_{px} \Delta x^2, \tag{7}$$

where N_{px} is the number of pixels for each cloud k. The mass flux per cloud m_k is computed as

$$m_k = \Delta x^2 \sum_{l}^{N_{\text{px}}} w_l \rho_l, \tag{8}$$

where ρ is density.

The identification of clouds and all subsequent calculations have to be done at a certain vertical level. Ideally, one would use the cloud base at the top of the boundary layer, since many convective parameterizations use the cloud base mass flux M_b as the input for their cloud models. There are, however, some complications. First, shallow convective clouds also occur at this level. These are typically ignored in parameterizations of deep convection, which is the focus of this study. Therefore, it makes sense to do the analysis above the shallow convective layer. Second, in our simulations of real weather, the height of the boundary layer, and therefore also the cloud base, varies temporally and spatially in the domain. Thus, our reasoning is to make sure that our chosen height is always above the boundary layer. Third, our studies have orography meaning that the height above sea level is variable. Due to this we chose to do our analysis on the terrain following model levels of the COSMO model (**?**), which in the lower troposphere closely follows the distance to the ground, but is basically parallel to the sea level height at the tropopause and above. The vertical profile of the domain average convective updraft mass flux is shown in Fig. 5 for the entire analysis domain, but also separately for Northern and Southern Germany at the time where the boundary layer is highest. Based on the reasoning laid out in this paragraph we chose model level 30 for our mass flux analyses, but in the Appendix also show the dependence of certain diagnostics with height.

3.2 Heating rate Q

To calculate statistics of the heating rate, the three dimensional field is summed in the vertical so that Q represents the total heating due to microphysics in the column.

3.3 Calculation of ensemble means and variances

For the variance calculations, a coarse-graining is applied to create coarse boxes $j = 1, ..., N_{\text{box,n}}$ with edge lengths of $n = 256, 128, 64, 32, 16, 8$ and $4\Delta x$, where $N_{\text{box,n}} = (256/n)^2$. No neighborhoods smaller are considered, since these would be significantly below the effective resolution of the model (Skamarock and Skamarock, 2004). The total mass flux per box per member $M_{i,j,n}$ is given by

$$M_{i,j,n} = \sum_{k=1}^{N_{\text{cld}\,i,j,n}} m_{k,i,j,n}. \tag{9}$$

To deal with clouds at the boundaries of the coarse-fields, the centers of mass for each cloud is first identified. Then the m_k is attributed to that one point in space. Therefore, the coarse box which contains the center of mass also contains the entire cloud, while the other box does not contain any of the cloud. $N_{i,j,n} = N_{\text{cld}\,i,j,n}$ is simply the number of clouds which fall into each box. This follows Cohen and Craig (2006). The heating rate per box is simply the average of all grid points in the box

Ensemble statistics of $\Phi = M, N, Q$ are then calculated for each box j. The sample variance is computed as

$$\langle(\delta\Phi)^2\rangle_{j,n} = \frac{1}{N_{\text{ens}}-1} \sum_{i=1}^{N_{\text{ens}}} (\Phi_{i,j,n} - \langle M\rangle_{j,n})^2, \tag{10}$$

where the ensemble mean is

$$\langle\Phi\rangle_{j,n} = \frac{1}{N_{\text{ens}}} \sum_{i=1}^{N_{\text{ens}}} \Phi_{i,j,n}. \tag{11}$$

To compute statistics for m a different approach is taken. Here the clouds in all members for each box are considered together to calculate the variance and mean. The total number of clouds over all ensemble members is denoted by $N_{\text{cldtot}} = \sum_{i=1}^{N_{\text{ens}}} N_{\text{cld}\,i,j,n}$.

$$\langle(\delta m)^2\rangle_{j,n} = \frac{1}{N_{\text{cldtot}}-1} \sum_{k=1}^{N_{\text{cldtot}}} (m_{k,j,n} - \langle m\rangle_{j,n})^2, \tag{12}$$

where the mean is

$$\langle m\rangle_{j,n} = \frac{1}{N_{\text{cldtot}}} \sum_{k=1}^{N_{\text{cldtot}}} m_{k,j,n}. \tag{13}$$

Since we are sampling a distribution with a limited number of data points N_{ens}, sampling issues arise when $\langle N\rangle$ becomes small ($\approx \frac{1}{N_{\text{ens}}}$). In particular, if only one member contains a cloud chances are that the real $\langle N\rangle < \frac{1}{N_{\text{ens}}}$ and we therefore overestimate the mean mass flux $\langle M\rangle$. To avoid this issue, a criterion is introduced where at least 5 out of 20 ensemble members must contain at least one cloud. *This threshold is a quick fix and should be determined statistically.*

Composites were computed by averaging over the 12 days in the simulation period. For the calculation of means (every overbar) and standard deviations (std), all coarse boxes at scale n for all ensemble members were first combined, and then the means and standard deviations were calculated. This ensures that, since the number of coarse boxes with clouds will differ from case to case, every coarse box is weighted equally.

4 Standard deviation versus mean

We now have a dataset containing values of $\langle M \rangle$, $\langle (\delta M)^2 \rangle$, $\langle Q \rangle$, $\langle (\delta Q)^2 \rangle$ for each coarsening scale n, grid box j and time t. The first goal of this study is to analyze the relation between the variability (in terms of the standard deviation or variance) and mean, and evaluate the theoretical predictions of CC06 and SPPT. Fig. 6a shows the standard deviation of M plotted against the mean for all times on a log-log plot. There seems to be a change in the relation somewhere between 10^7 and 10^8 kg/s, which is roughly the mean mass flux of an individual cloud m. This indicates that this change in the slope could be a sampling issue. To evaluate whether a linear relation between the standard deviation and the mean (SPPT) or a square root relation (CC06) fits our data better least square fits of $y = b * x$ and $y = \sqrt{b * x}$ were done, respectively. The corresponding fits are displayed as lines, while the fit parameter b and the normalized root mean square error of the fit are shown in Fig. 6b. What is immediately evident is the scale dependence of the fit parameter b for the SPPT prediction, which drops from around 1.5 to 0.1 going towards larger scales. The fit parameter for the square root CC06 prediction, on the other hand, stays relatively constant with values ranging from 0.8–1.25x10^8. The quality of the fit as measured by the NRMSE is smaller for most n for the CC06 predictions, particularly for medium n. These results suggest that for M, the relation between the variability and mean is better described by the CC06 theory than by the SPPT theory. In particular the CC06 theory is scale adaptive, while the random parameter for SPPT has to be adapted to the grid size.

Do these findings also apply to Q. In other words, we are asking whether there is a clear correlation between the means and standard deviations of Q and M. Since M is a summed quantity while Q is an average quantity, Q is first multiplied by the area of the coarse box $A = n^2$ to make the two quantities comparable between scales. The correlation coefficient is shown in Fig. 6d. For the standard deviation the correlation coefficient is greater 0.9 for all n except the smallest scale. For the means the correlation is not as good, particularly for the largest scale where the correlation coefficient drops to 0.65. Still, the two quantities are related. One big difference between M and Q, as they are used in this study, is that $\langle Q \rangle$ can be zero or negative, while there is a lower limit for M.

Where do negative values come from. Could they be related to non-zero M? Should I show or mention the fit quality for Q as well?

4.1 Testing the assumptions of CC06

While the CC06 theory seems to predict the variability of the convective mass flux and heating rates reasonably well, there are still significant fluctuations. We will now attempt to look at all the assumptions made in deriving EQ. In particular, (a) m is constant, (b) the mass flux per cloud is distributed exponentially, (c) clouds are distributed randomly resulting in a Poisson distribution for N, and (d) the cloud number N and cloud mass flux m are uncorrelated.

Assumption (a) is not an assumption made by CC06 where $\langle m \rangle$ is an input parameter for the prediction of the variance. It is however an assumption made in PC08. Fig. 7a shows the temporal evolution of the mean mass flux $\langle m \rangle$. The composite mean is relatively constant at around 5x10^7 kg/s. This is around twice the value diagnosed by Cohen and

Craig (2006) and used in PC08. There are however significant day-to-day fluctuations and some days show a quite strong diurnal cycle with values ranging from 2–7x10^7 kg/s.

Assumption (b), namely the exponential distribution of m is at the core of the CC06 theory and the PC08 parameterization. Fig. 7 shows histograms of cloud size and m for all times and combined for all days. While both distributions largely follow an exponential distribution there are some deviations. One measure is the parameter $\beta = \langle (\delta m)^2 \rangle / \langle m \rangle^2$, which should be 1. For the cloud size distribution this parameters is 0.77 while for the mass flux distribution it is 1.20 indicating a broader distribution. *Does it make sense to look at the correlation between m and cloud size as another assumption?* Fig. 8? shows the temporal evolution of β evaluated for each scale n. β depends significantly on scale with larger values, i.e. broader distributions, for larger scales. This issue will be explored later. The diurnal variation of β is on the order of 10% and corresponds with the diurnal variation of the mean cloud mass flux.

Assumption (c), namely the random (Poisson) distribution of the cloud number N, can be tested by the parameter $\alpha = \langle (\delta N)^2 \rangle / \langle N \rangle$ which should be one. Larger values indicate a preferred occurrence of clouds near already existing clouds (we will call this process clustering), while values smaller than 1 indicate a more regular spatial distribution of clouds. Fig. 8? shows the temporal evolution of α for each scale. A diurnal cycle is evident for all scales, which is strongest for the medium and large n. In particular, there seems to be a minimum in clustering during the convective peak at around 13UTC and then strongly increasing clustering from 15UTC to 20UTC. A different measure for clustering is the radial distribution function shown in Fig. 10. For all times there seems to be clustering which is strongest at a distance of around 25 km, crossing below 1 at around 100 km. The diurnal variation of the RDF is in accordance with α, particularly an increased clustering towards the evening hours.

To get a quantitative measure of how important the violations of the assumptions discussed in the two previous paragraphs are, the root mean square error of the relative deviation from the theory is calculated. Then α and β are taken into account and the reduction of the error is considered (Fig. 11). For the medium and large scales the clustering as indicated by α has the strongest effect and for medium n explains almost half of the deviations. For the smallest n the β parameter is in fact very important. Accounting for both parameters around half of the deviations for small and medium n can be explained, while a large portion of the error for large scales remains.

In particular, while for small and medium scales on average the adjusted prediction fits the simulation data very well, there is a significant bias for larger scales where the variability is overpredicted. The remaining assumption (d) is that the cloud mass flux and the number of cloud are uncorrelated. From Fig. 7 a temporal correlation between the two variables can be assumed. *Is this enough of an explanation of should we look deeper into the correlation of the two?*

In particular the large diurnal cycle of clustering can cause the variability estimates to have error on the order of 50%. This suggest that in order to improve the estimates clustering should in some way be included in the theoretical model of convection. There are two main challenges which arise: (a) finding a simple model of convection with clustering and (b) finding some GCM grid-scale predictor for clustering which can then be passed as a parameter to the simple model.

—

Fig. ??? shows the relation between the means and variances of M and Q and the correlation between the mass flux and heating rates. The correlation coefficient between M and Q is typically above 80% except for large n, while for the standard deviations the correlation is always good. This indicates that even though M only includes updrafts, these are still representative for most of the heating due to microphysics. In panels a) and b) two lines are drawn, representing the CC06 prediction using a value for $\langle m \rangle = 0.6e8$, which is close to the overall mean and using $1/12$ as the slope for the SPPT prediction based on current settings at ECWMF.

M and Q std vs mean with line for CC06, SPPT and best fit function for all times.

Some diurnal cycle plot. with alpha I guess, maybe beta, not sure what to do about it...

Here probably also RDF.

A radial distribution function (RDF) is calculated at each time for each member separately. To do this, the center of mass for each cloud is identified. For these points a two-dimensional pair correlation is computed, where the step size of the search function is $2\Delta x$ and the maximum search radius is $30\Delta x$. The output is normalized, so that a completely randomly distributed field would give an RDF of 1 at all radii. The results are averaged over the ensemble members to give one RDF at each time. A sketch of how the RDF is calculated is given in Fig. **??** (right).

5 A simple clustering model

As we have seen from the results so far clustering of clouds is the biggest factor for modulating convective variability. In this section a simple cloud model will be used with the goal to explain most of the deviations.

Explain Julia's model.

For each time, get the crs which fits best given M and m as an input and var(M) as the output. Then show the diurnal cycle of crs.

6 Can we find a large-scale predictor for crs.

HPBL, dtM

7 Conclusion

References

Bengtsson, L., M. Steinheimer, P. Bechtold, and J.-F. Geleyn, 2013: A stochastic parametrization for deep convection using cellular automata. *Quarterly Journal of the Royal Meteorological Society*, **139 (675)**, 1533–1543, doi:10.1002/qj.2108, URL: http://doi.wiley.com/10.1002/qj.2108.

Cohen, B. G. and G. C. Craig, 2006: Fluctuations in an Equilibrium Convective Ensemble. Part II: Numerical Experiments. *Journal of the Atmospheric Sciences*, **63 (8)**, 2005–2015, doi: 10.1175/JAS3710.1, URL: http://journals.ametsoc.org/doi/abs/10.1175/JAS3710.1.

Craig, G. C. and B. G. Cohen, 2006: Fluctuations in an Equilibrium Convective Ensemble. Part I: Theoretical Formulation. *Journal of the Atmospheric Sciences*, **63 (8)**, 1996–2004, doi: 10.1175/JAS3709.1, URL: http://journals.ametsoc.org/doi/abs/10.1175/JAS3709.1.

Davies, L., 2008: Self-organisation of convection as a mechanism for memory. Ph.D. thesis.

Davoudi, J., N. A. McFarlane, and T. Birner, 2010: Fluctuation of Mass Flux in a Cloud-Resolving Simulation with Interactive Radiation. *Journal of the Atmospheric Sciences*, **67 (2)**, 400–418, doi:10.1175/2009JAS3215.1, URL: http://journals.ametsoc.org/doi/abs/10.1175/2009JAS3215.1.

Done, J. M., G. C. Craig, S. L. Gray, P. a. Clark, and M. E. B. Gray, 2006: Mesoscale simulations of organized convection: Importance of convective equilibrium. 737–756, doi:10.1256/qj.04.84, URL: http://centaur.reading.ac.uk/5286/.

Dorrestijn, J., et al., 2015: Stochastic Parameterization of Convective Area Fractions with a Multicloud Model Inferred from Observational Data. *Journal of the Atmospheric Sciences*, **72 (2)**, 854–869, doi:10.1175/JAS-D-14-0110.1, URL: http://journals.ametsoc.org/doi/10.1175/JAS-D-14-0110.1.

Dorrestijn, J., et al., 2016: Stochastic Convection Parameterization with Markov Chains in an Intermediate-Complexity GCM. *Journal of the Atmospheric Sciences*, **73 (3)**, 1367–1382, doi:10.1175/JAS-D-15-0244.1, URL: http://journals.ametsoc.org/doi/10.1175/JAS-D-15-0244.1.

Flack, D. L. A., R. S. Plant, S. L. Gray, H. W. Lean, C. Keil, and G. C. Craig, 2016: Characterisation of Convective Regimes over the British Isles. *Quarterly Journal of the Royal Meteorological Society*, n/a–n/a, doi:10.1002/qj.2758, URL: http://doi.wiley.com/10.1002/qj.2758.

Gottwald, G. A., K. Peters, and L. Davies, 2016: A data-driven method for the stochastic parametrisation of subgrid-scale tropical convective area fraction. *Quarterly Journal of the Royal Meteorological Society*, **142 (694)**, 349–359, doi:10.1002/qj.2655, URL: http://doi.wiley.com/10.1002/qj.2655.

Kober, K., G. C. Craig, K. Kober, and G. C. Craig, 2016: Physically Based Stochastic Perturbations (PSP) in the Boundary Layer to Represent Uncertainty in Convective Initiation. *Journal of the Atmospheric Sciences*, **73 (7)**, 2893–2911, doi:10.1175/JAS-D-15-0144.1, URL: http://journals.ametsoc.org/doi/10.1175/JAS-D-15-0144.1.

Plant, R. S. and G. C. Craig, 2008: A Stochastic Parameterization for Deep Convection Based on Equilibrium Statistics. *Journal of the Atmospheric Sciences*, **65 (1)**, 87–105, doi:10.1175/2007JAS2263.1, URL: http://journals.ametsoc.org/doi/abs/10.1175/2007JAS2263.1.

Skamarock, W. C. and W. C. Skamarock, 2004: Evaluating Mesoscale NWP Models Using Kinetic Energy Spectra. *Monthly Weather Review*, **132 (12)**, 3019–3032, doi: 10.1175/MWR2830.1, URL: `http://journals.ametsoc.org/doi/abs/10.1175/MWR2830.1`.

Taylor, H. and S. Karlin, 1998: *An introduction to stochastic modeling*. URL: `https://books.google.de/books?hl=en&lr=&id=ppHiBQAAQBAJ&oi=fnd&pg=PP1&dq=An+Introduction+t`

Wang, Y., G. J. Zhang, and G. C. Craig, 2016: Stochastic convective parameterization improving the simulation of tropical precipitation variability in the NCAR CAM5. *Geophysical Research Letters*, **43 (12)**, 6612–6619, doi:10.1002/2016GL069818, URL: `http://doi.wiley.com/10.1002/2016GL069818`.
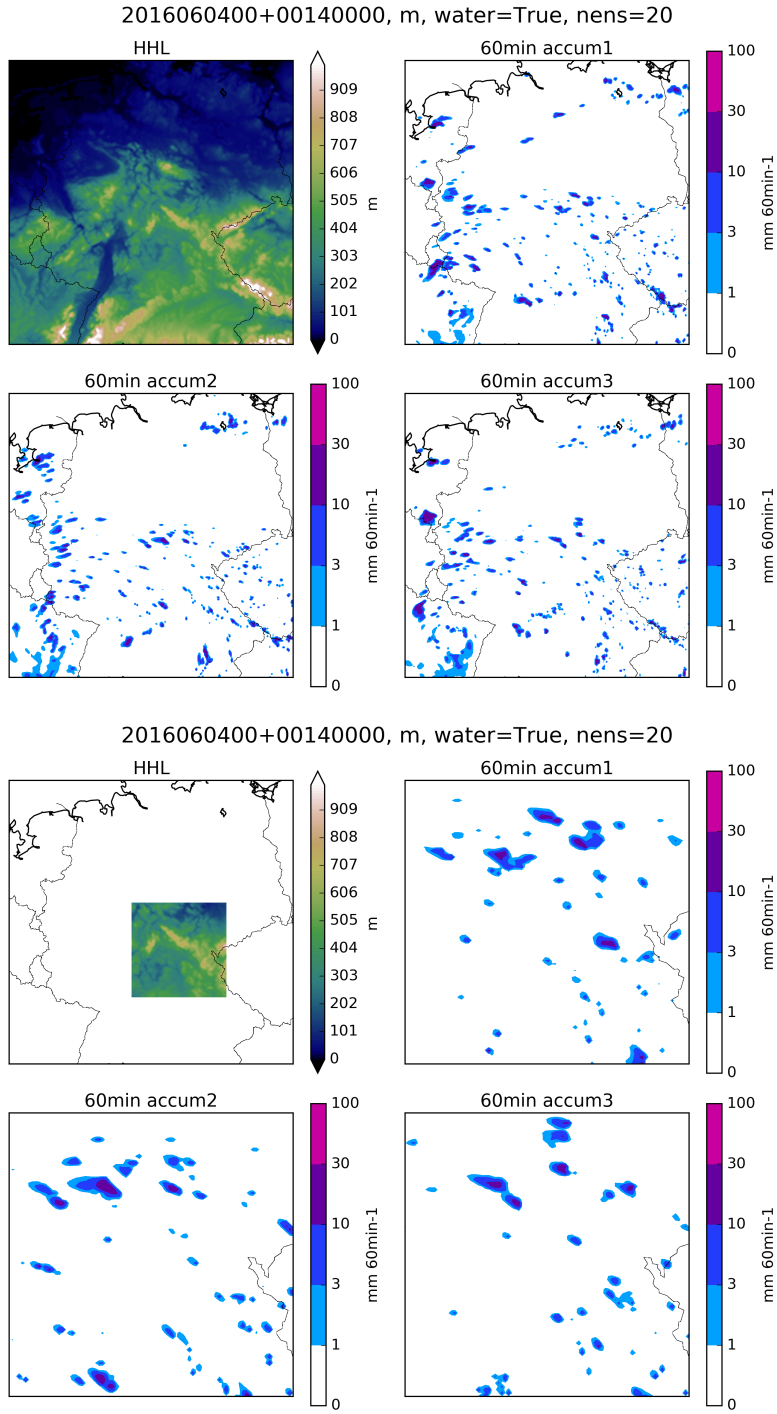
8   Figures

Figure 2: (a) Surface elevation of the analysis domain. (b–d) Precipitation fields of three ensemble members for DATE. Bottom plots show a zoom.
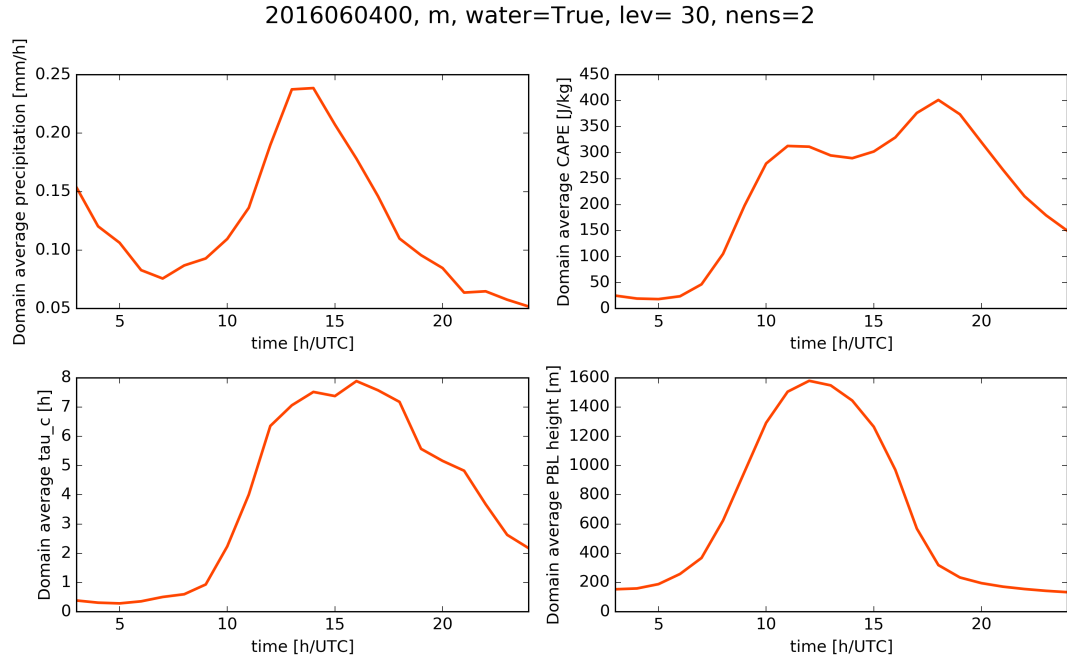
Figure 3: Time series of (a) hourly rainfall in mm/h, (b) CAPE in J/kg, (c) the convective adjustment time scale in h and (d) the perturbed boundary layer height in m. All values are domain and ensemble averages. Each gray line represents one simulation day. The red line is the mean over all simulation days.
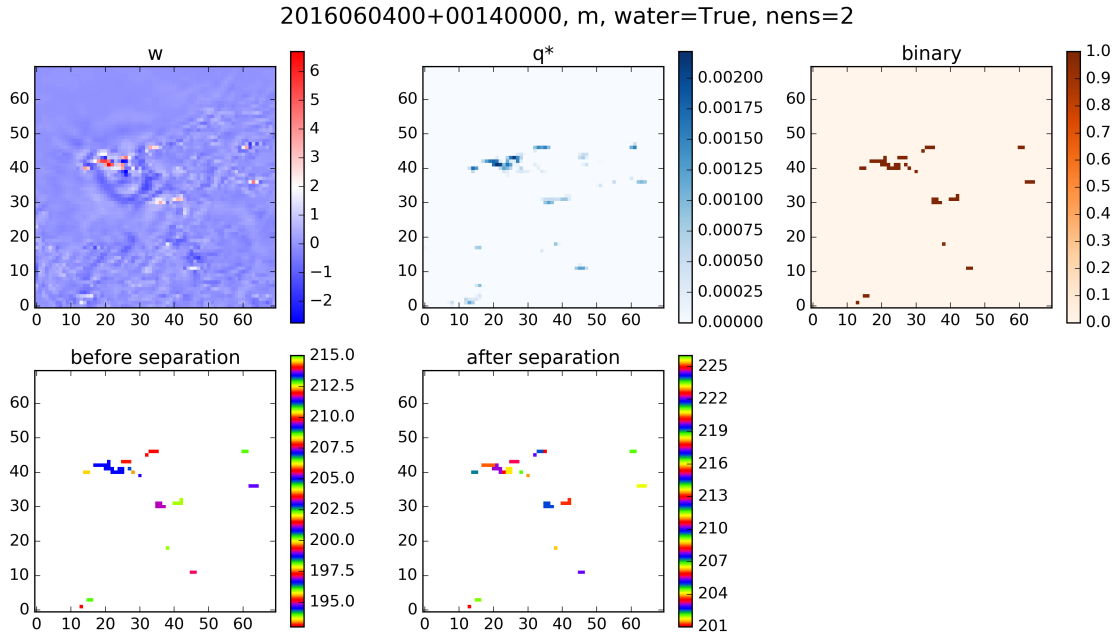
Figure 4: Cloud identification algorithm. First, a binary field (c) is created by applying thresholds to the vertical velocity (a) and cloud water (b) fields. Then, the contiguous clouds are identified (d), followed by a separation using a local maximum and watershed method (e)

15
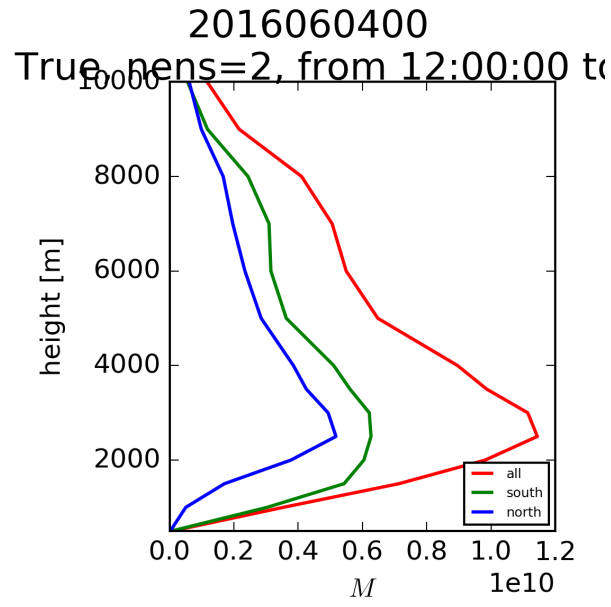
Figure 5: Vertical mass flux profile for the total domain (average surface height: 247 m) and the Northern (79 m) and Southern (415 m) part of the domain.
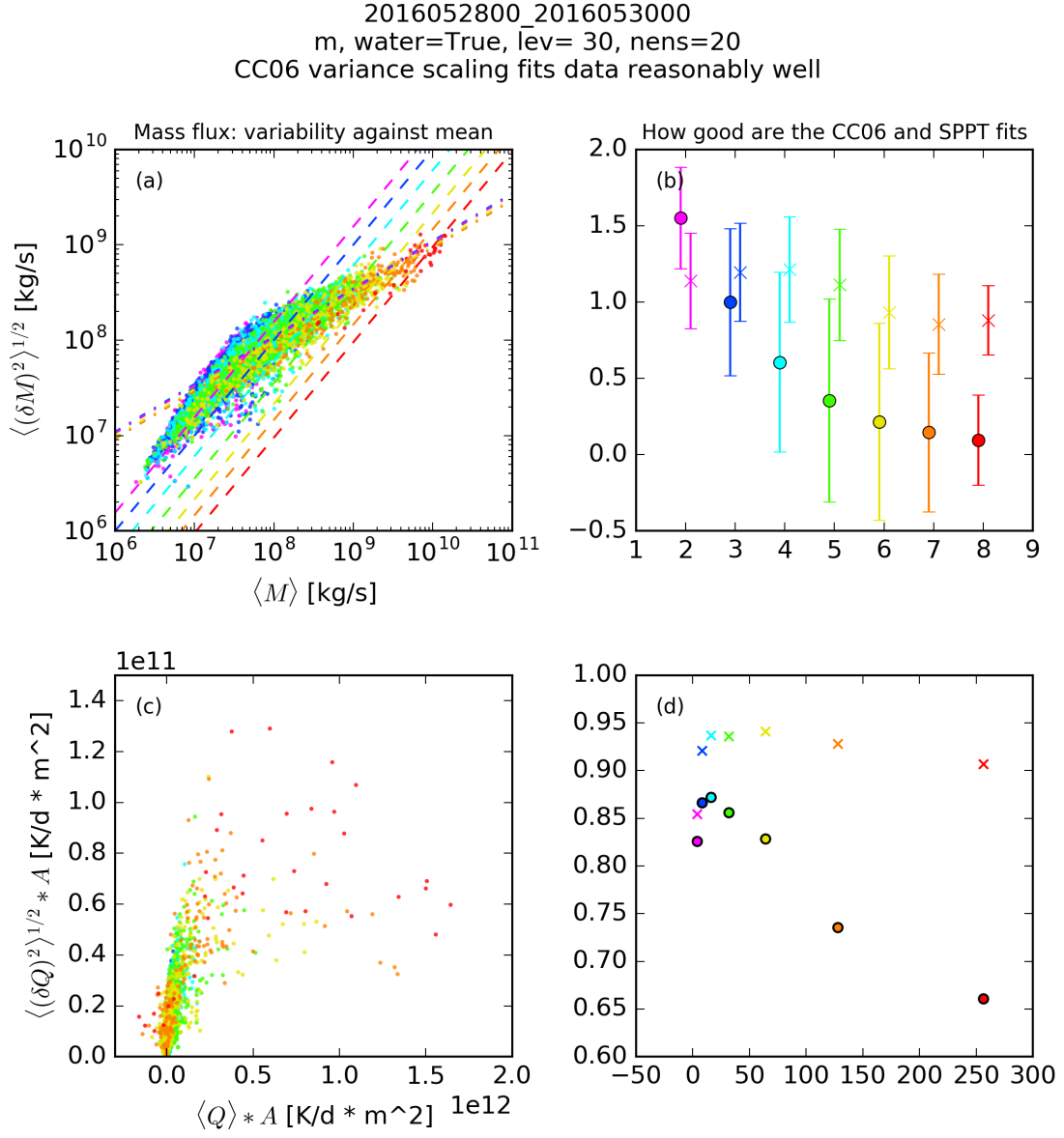
Figure 6: (a) Standard deviation of M plotted against mean. (b) Fitting parameters for CC06 and SPPT along with normalized RMSE. (c) Standard deviation of $Q * A$ plotted against mean. (d) Correlation coefficient of means and standard deviations of M and Q.
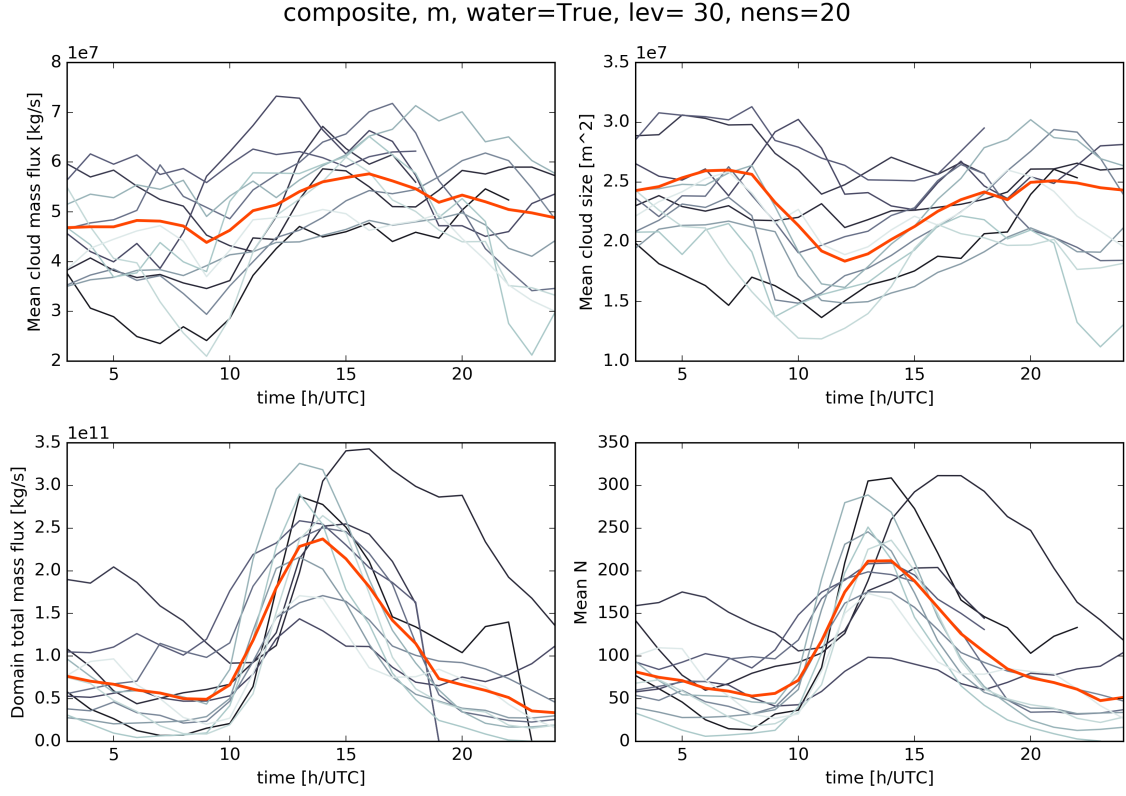
Figure 7: (a) Temporal evolution of the domain mean m, (b) cloud size, (c) domain total mass flux M and (d) cloud number N.
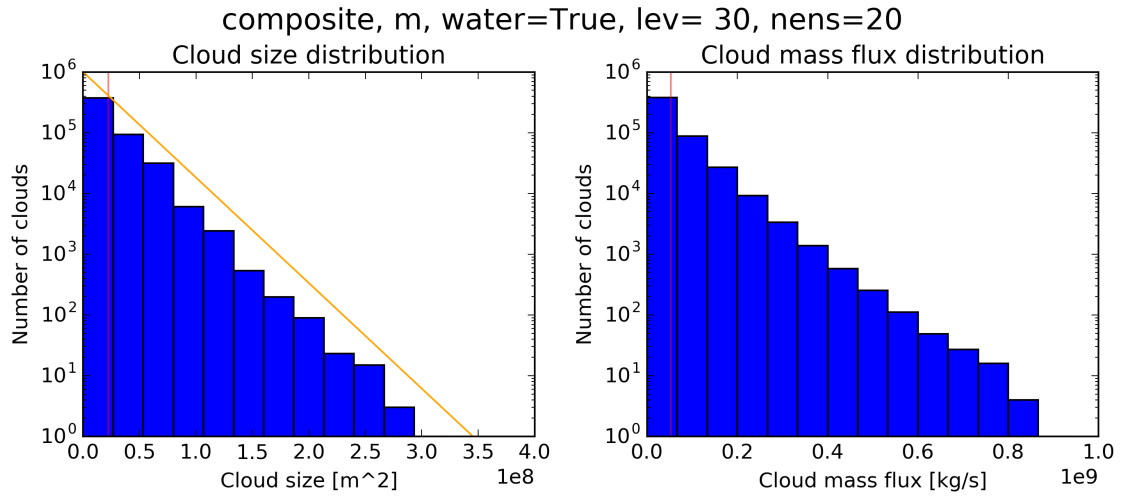
Figure 8: (a) Distribution of cloud size and (b) cloud mass flux. For all times and cases.

18
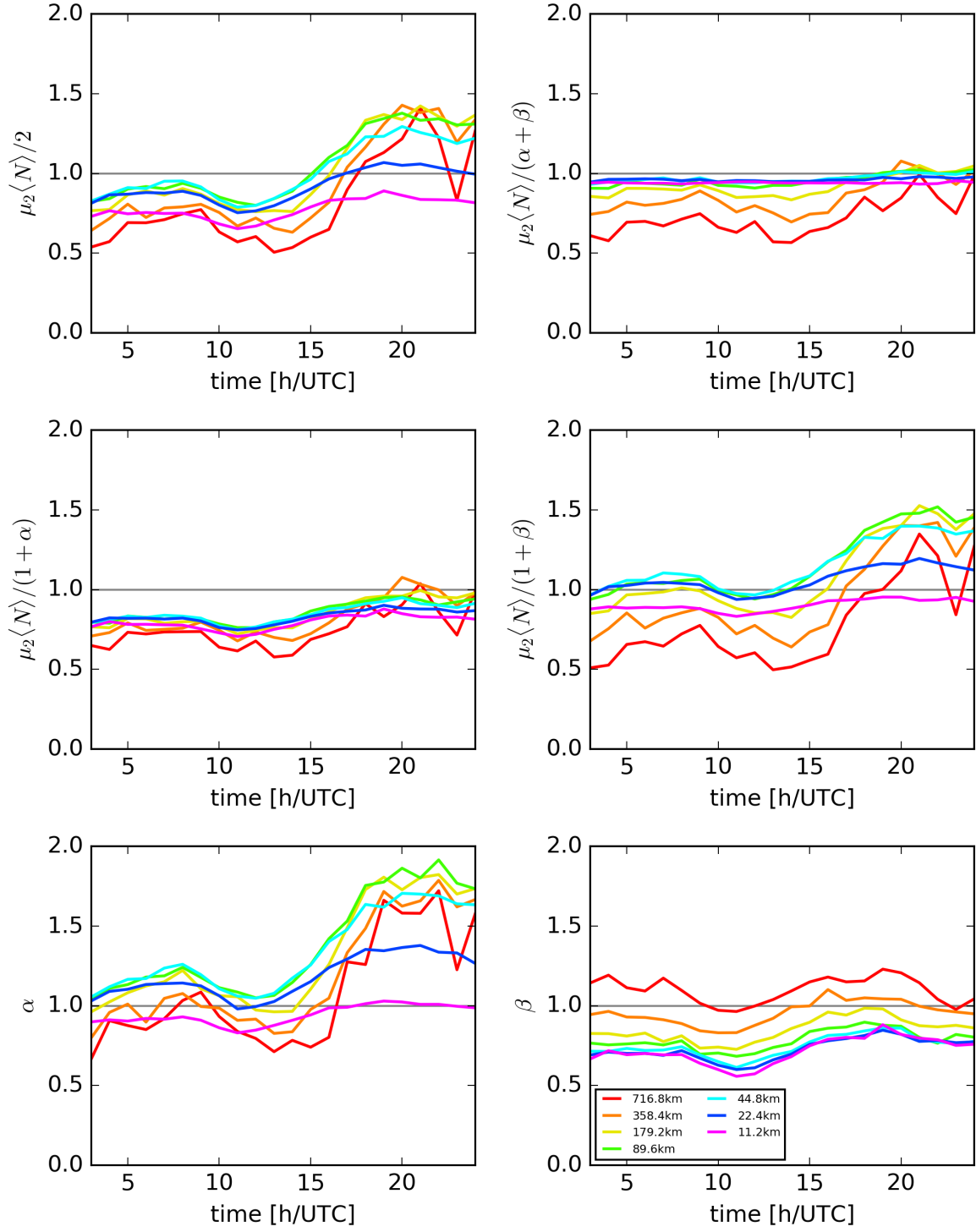
Figure 9: Time evolution for the mean of several variables.

composite
lev= 30, nens=20
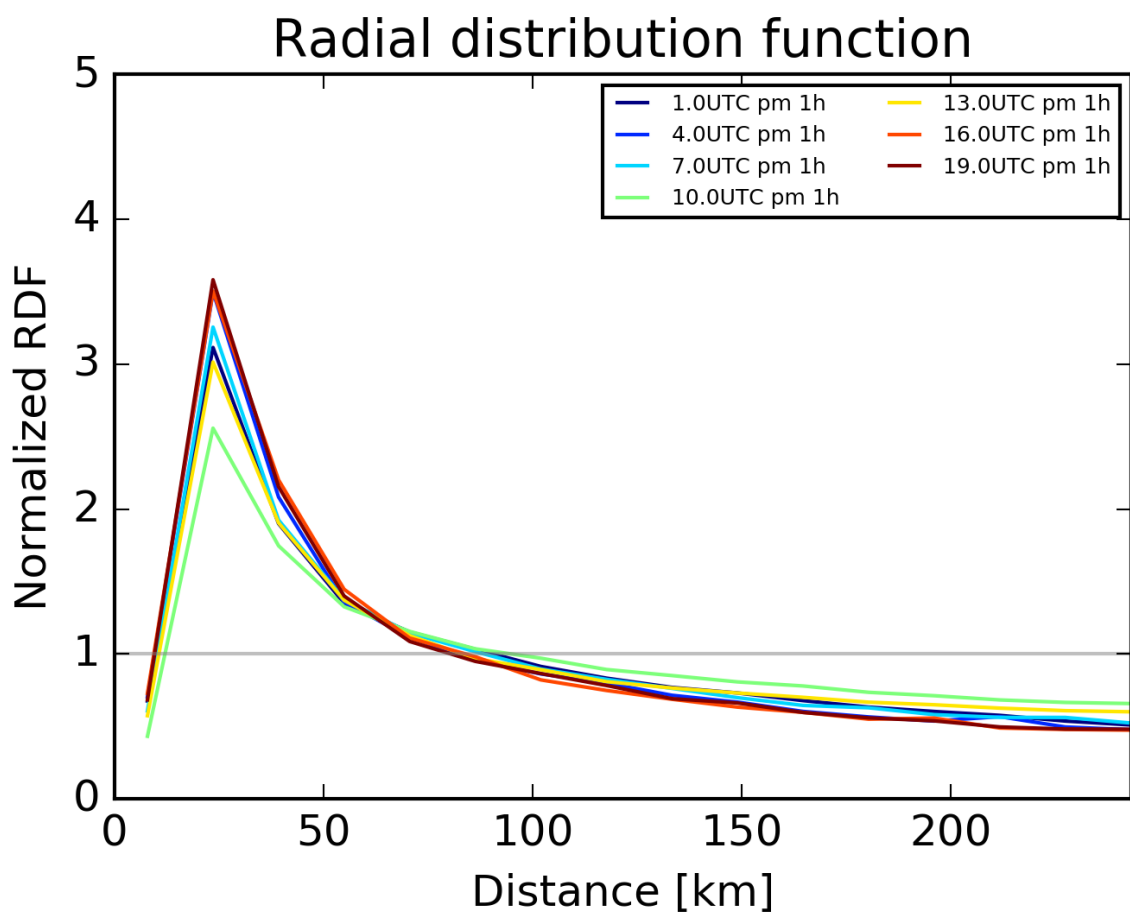
Radial distribution function

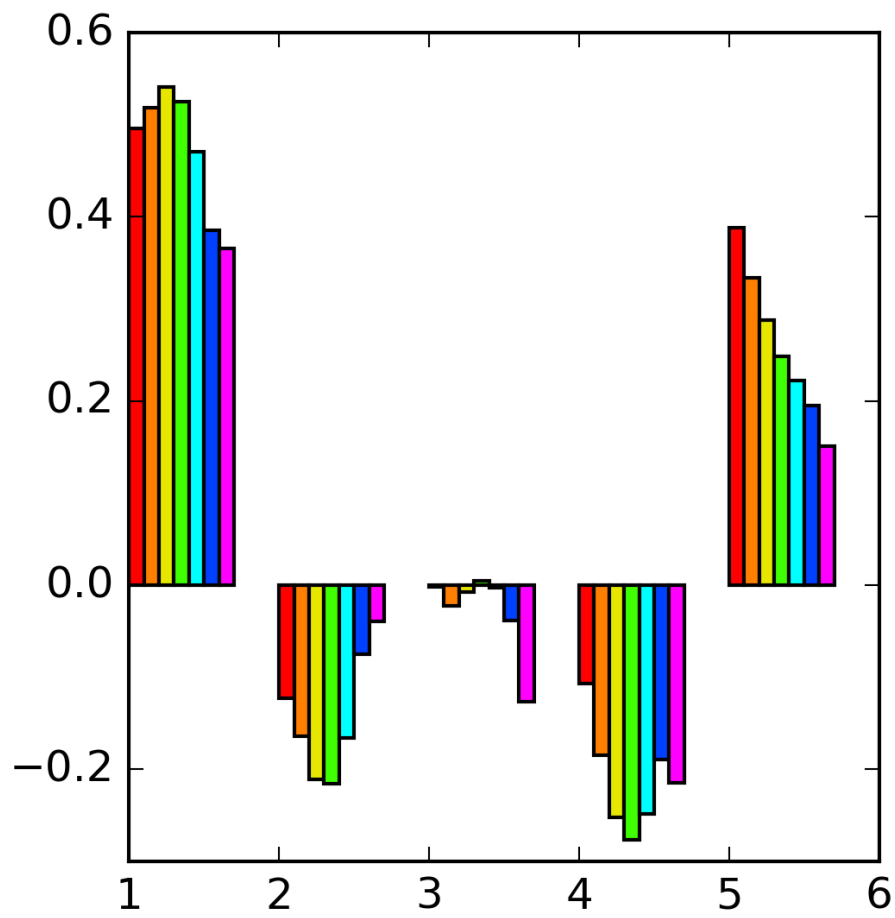Figure 10: As above but for the composite.

Figure 11: Scatter plots for several variables. Small dots for each j, n is denoted by different colors. The large dots represent the mean values for each n.